Electronic Supplementary Material (ESI) for ChemComm.

Supplementary Information

for

A Highly Substituted Pyrazinophane Generated from a Quinoidal System via a Cascade Reaction

Christopher L. Anderson,[a,b] Jiatao Liang,[a,b] Simon J. Teat,[c] Andrés Garzón-Ruiz,[e] David P. Nenon,[b,d] Amparo Navarro,[f] Yi Liu*[a]

[a]The Molecular Foundry, [c]Advanced Light Source, and [d]Materials Sciences Division, Lawrence Berkeley National Laboratory, One Cyclotron Road, Berkeley, California 94720, United States

[b]Department of Chemistry, University of California, Berkeley, Berkeley, California 94720, United States

[e]Department of Physical Chemistry, Faculty of Pharmacy, Universidad de Castilla-La Mancha, Cronista Francisco Ballesteros Gómez, 02071 Albacete, Spain

[f]Department of Physical and Analytical Chemistry, Faculty of Experimental Sciences, Universidad de Jaén, Paraje las Lagunillas, 23071 Jaén, Spain

Corresponding Author: Yi Liu, E-mail: yliu@lbl.gov.

The Molecular Foundry, 67 Cyclotron Rd, Lawrence Berkeley National Labs, Berkeley, CA 94720

Page	Contents
2 - 5	Experimental Procedures: General, X-ray Crystallography, Synthesis
5	Figure S1: Additional Computed Orbital Density Diagrams of Compounds **4**, **5**, and **6**
6	Table S1: Computed Energies of Lowest-Energy Conformers of Compounds **5**, **6**, and **7**
6	Figure S2: Additional Computational Details on pseudo-ortho and pseudo-geminal versions of **5**
7	Figure S3: Visualizations of Lowest-Energy Conformers of Compounds **5**, **6**, and **7**
8	Table S2: Summary of Relevant Information on the Computed Absorption of Compounds **5**, **6**, and **7**
8	Table S3: Summary of Relevant Information on the Computed Fluorescence of Compounds **5**, **6**, and **7**
8	Figure S4: Representation of Pertinent Bond Lengths in Compound **5** in the Ground and Excited States
9	Figure S5: Thermogravimetric Analysis (TGA) Traces of the Compound **5**
9	Figure S6: Differential Scanning Calorimetric (DSC) Traces of Compound **5**
10	Figure S7: Additional Experimental and Calculated UV-Visible and Fluorescence Spectroscopy of **5**, **6**, and **7**
11	Figure S8: UV-Visible Spectroscopy of Different Concentrations of **5**, **6**, and **7**
12	Figure S9: Fluorescence Lifetime Traces for Compounds **5**, **6**, and **7**
12	Figure S10: X-ray Crystallographic Structure of Compound **6**
13 - 26	Figures S11 - S24: Nuclear Magnetic Resonance (NMR) Spectra of All Herein Reported Compounds
27	Supporting Information References

Experimental Procedure

General

All reactions were carried out in oven-dried glassware sealed with rubber septa under an atmosphere of nitrogen unless otherwise noted and were stirred using Teflon-coated magnetic stir bars. Large volumes of volatile solvents were removed using rotary evaporation, and small volumes of volatile solvents were removed using nitrogen gas flow. All commercially-available chemicals were purchased from Alfa Aesar, Spectrum Chemicals, Acros Organics, TCI America, or Sigma-Aldrich, and were used without further purification. Deuterated solvents were purchased from Cambridge Isotope Laboratories and used as received. All NMR spectra were recorded at 298 K unless otherwise specified on a Bruker 500 MHz Avance instrument. All chemical shifts are quoted using the δ scale, and all coupling constants (J) are expressed in Hertz (Hz). ^{1}H and ^{13}C NMR spectra chemical shifts are reported relative to the residual solvent signal (^{1}H NMR: $CDCl_3$ δ = 7.26 ppm and DMSO-d_6 δ = 2.50 ppm; ^{13}C NMR: $CDCl_3$ δ = 77.16 ppm and DMSO-d_6 δ = 39.52 ppm) and ^{19}F NMR spectra chemical shifts are reported relative to hexafluorobenzene added as an internal standard (C_6F_6 = -164.9 ppm).[1] NMR data are reported as follows: chemical shift (multiplicity, coupling constants where applicable, number of hydrogens where applicable). Splitting is reported with the following symbols: s = singlet, d = doublet, t = triplet, dd = doublet of doublets, td = triplet of doublets, ddd = doublet of doublet of doublets, sept = septet, m = multiplet. MALDI-TOF mass spectrometry experiments were performed on an Applied Biosystems 4800 MALDI TOF/TOF instrument in reflector mode using super-DHB (purchased from Sigma-Aldrich) as matrix. UV-Vis-NIR spectra were recorded using a Cary 5000 UV-Vis-NIR spectrometer. Each spectrum was taken in a dilute solution in dichloromethane. Differential scanning calorimetry was performed using a TA Instruments DSC Q2000 and thermogravimetric analysis was performed on a TA Instruments TGA 5500. Time-resolved fluorescence lifetimes were collected on a Picoquant Fluotime 300 with PMA 175 detector and an LDH-P-C-280 diode laser (excitation wavelength of 280 nm). Each spectrum was taken in a dilute solution in dichloromethane. All fits were performed with FluoFit software. The instrument response function (IRF) was measured by scattering from a glass cover slip. Absolute quantum yields were determined optically using a home-built integrating sphere spectrofluorometer. A Fianium SC450 supercontinuum pulsed laser is used as a white-light source. The desired excitation wavelength is selected using an excitation monochromator, and a small part of this excitation is directed to a ThorLabs S120VC calibrated silicon photodiode to measure the power, while the remainder is directed to a Spectralon integrating sphere from LabSphere, where it strikes a cylindrical cuvette containing the sample. The remaining light, which is a mixture of laser light and sample luminescence, eventually exits the integrating sphere and is focused onto an emission monochromator and the spectrum is detected using a thermoelectrically cooled Princeton Instruments PIXIS 400B CCD. The CCD is calibrated with a NIST-traceable radiometric calibration lamp. A complete description of this home-built integrating sphere spectrofluorometer can be found elsewhere.[2]

Computational Details

Computations run using the B3LYP functional were run on the Etna partition of the Lawrence Berkeley National Labs Supercluster using Qchem 5.1.[3] Molecular geometries were optimized starting from structures generated in the IQmol software and relaxed using the UFF molecular mechanics force field.[4] Molecular geometries were then optimized and single-point energies were determined at the 6-311++G** level using the B3LYP functional. Orbital density maps were visualized using the IQmol software with an isovalue of 0.02.

Computations run using the PBE0 functional were performed using the Gaussian09 (revision D.01) suite of programs Geometric optimization and single-point energies were found using the PBE0 functional in combination with the 6-31G* basis set.[5-7] A conformational analysis in the gas phase was carried out for compounds **5**, **6**, and **7** in order to find the most energetically stable conformer. The lowest-energy gas-phase conformers of these compounds were then employed as the starting points in ground state geometry-optimizations in dichloromethane solution using the Polarizable Continuum Model (PCM).[8-10] The vertical electronic transitions of compounds **5**, **6**, and **7** were calculated with dichloromethane as the solvent, and the harmonic vibrational frequencies were computed to check for the absence of imaginary vibrational frequencies.The reaction of compound **4** to form the dimeric **5** was modeled including solvent effects (with *p*-xylene as the solvent). The vertical electronic transitions (absorption and emission) and the geometry of the first excited state (S_1) of **5**, **6**, and **7** were computed using time dependent (TD)-DFT (TD-PBE0/6-31G*) within the linear response regime. The PBE0 hybrid exchange-correlation functional has shown to be suitable to estimate the singlet excited state of organic molecules in the extensive TD-DFT benchmark reported by Jacquemin et al.[11] The fluorescence emission energy was calculated as

$$\Delta E_{em} = E_{S1}(G_{S1}) - E_{S0}(G_{S1}) \quad (1)$$

where $E_{S1}(G_{S1})$ is the energy of the S_1 state at its equilibrium geometry (in the SS solvation approach) and $E_{S0}(G_{S1})$ is the energy of the S_0 state at the S_1 state geometry and with the static solvation from the excited state.

X-ray Crystallography

Compounds were crystallized via dissolution in 1 mL of tetrahydrofuran in a 2-dram vial with the vial cap slightly unscrewed. After 1 week undisturbed, compounds **5** and **6** had formed yellow and white crystals, respectively, roughly 0.5 mm in size of suitable quality to obtain x-ray structures. Single crystals of **5** and **6** were selected and mounted on Mitegen® loops with Paratone oil, and data were collected on beamline 11.3.1 at the Advanced Light Source with λ = 0.7749 Å at 100 K using an Oxford Cryosystems Cryostream 700 plus. The x-ray structures of compounds **5** and **6** were collected on a Bruker D8 diffractometer with a Bruker PHOTON100 CMOS detector. Data reduction was performed and corrected for Lorentz and polarization effects using SAINT[12] v8.38a and were corrected for absorption effects using SADABS v2016/2[13]. Structures were solved using SHELXT[14] using the direct method and were refined by least-square refinement against F^2 by SHELXL[15].

Synthesis

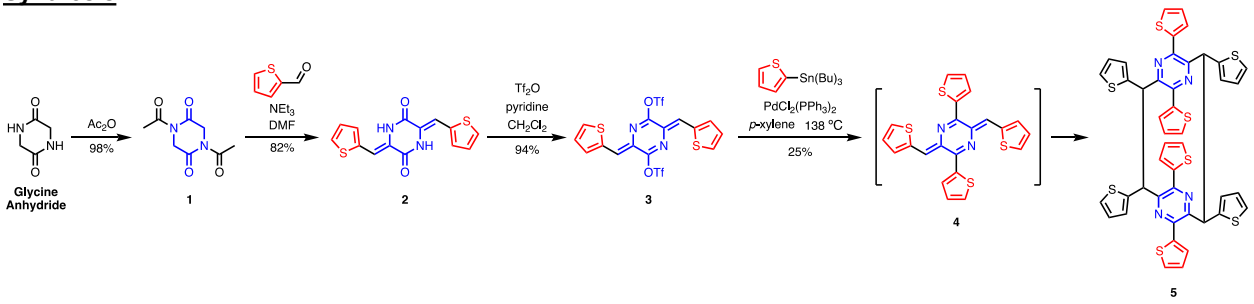

1,4-Diacetylpiperazine-2,5-dione (**1**)
1,4-Diacetylpiperazine-2,5-dione was synthesized from glycine anhydride according to a previously reported procedure.[16]

Compound **2**
Compound **2** was synthesized from 1,4-diacetylpiperazine-2,5-dione according to a previously reported procedure.[17] 1,4-Diacetylpiperazine-2,5-dione (**1**) (25.23 mmol, 5.00 g), triethylamine (100.92 mmol, 14.08 mL), and thiophene-2-carboxaldehyde (55.51 mmol, 5.19 mL) were dissolved in DMF (50 mL), and the resulting solution was stirred at 120 °C for 15 h. The reaction mixture was then cooled to room temperature and diluted with water (50 mL). The

precipitated solid was filtered and washed with water, ethyl acetate, and methanol to afford compound **2** as a fluffy yellow powder (82%). ^{1}H NMR (500 MHz, DMSO-d_6) δ 9.89 (s, 1H), 7.74 (d, J = 5.0 Hz, 1H), 7.57 (d, J = 3.7 Hz, 1H), 7.19 (dd, J = 5.1, 3.7 Hz, 1H), 6.97 (s, 1H). ^{13}C NMR (126 MHz, DMSO-d_6) δ 158.36, 136.00, 130.60, 129.01, 128.81, 124.82, 109.34. MS (MALDI-TOF) for $C_{14}H_{10}N_2O_2S_2$ $[M]^+$: calcd., 302.0184; found, 301.9622.

Compound **3**

Compound **3** was synthesized from **2** according to a previously reported procedure.[17] Trifluoromethanesulfonic anhydride (neat, 21.33 mmol, 3.58 mL) was added dropwise to a solution of compound **2** (9.92 mmol, 3.00 g) and pyridine (19.84 mmol, 1.60 mL) in dichloromethane (50 mL) at -78 ºC (dry ice/acetone bath). The reaction was stirred at -78 ºC for 30 mins and then slowly warmed to room temperature and stirred over 16 h. Hexanes was added to the crude reaction mixture, the precipitate was filtered, and the filtrate was washed with hexanes, water, and methanol to give analytically pure product as red-orange flakes (94%). ^{1}H NMR (500 MHz, $CDCl_3$) δ 7.73 (d, J = 5.1 Hz, 1H), 7.55 (d, J = 3.8 Hz, 1H), 7.18 (s, 1H), 7.15 (dd, J = 5.1, 3.8 Hz, 1H). ^{13}C NMR (126 MHz, $CDCl_3$) δ 150.70, 137.12, 136.25, 135.93, 127.82, 124.34, 123.82. MS (EI) for $C_{16}H_8F_6N_2O_6S_4$ $[M]^+$: calcd., 565.9169; found, 565.9165.

Compound **5**

To a solution of bis(triphenylphosphine)palladium(II) dichloride (0.011 g, 0.016 mmol) in *p*-xylene (4 mL) was added compound **3** (0.100 g, 0.177 mmol) and 2-(tributylstannyl)thiophene (0.22 mL, 0.71 mmol). The mixture was stirred at 138 ºC for 4 h before being cooled to room temperature. The reaction solution was filtered and washed through with dichloromethane (10 mL). The solvent was evaporated *en vacuo* and the residue was purified via column chromatography (hexanes to dichloromethane gradient) to give a canary yellow powder (0.019 g, 0.04372 mmol, 25% yield). ^{1}H NMR (500 MHz, $CDCl_3$) δ 7.35 (dd, J = 5.00, 0.95 Hz, 2H), 7.34 (dd, J = 3.70, 1.00 Hz, 2H), 7.29 (dd, J = 5.05, 1.10 Hz, 2H), 7.08 (dd, J = 3.45, 1.15 Hz, 2H), 7.06 (dd, J = 4.98, 3.73 Hz, 2H), 7.00 (dd, J = 5.10, 3.50 Hz, 2H), 5.26 (s, 2H) ppm; ^{13}C NMR (125 MHz, $CDCl_3$) δ 143.00, 142.46, 141.39, 139.49, 129.01, 128.08, 128.03, 127.07, 126.78, 125.76 ppm, 54.83 ppm; MS (MALDI-TOF) for $C_{22}H_{16}N_2S_4$ $[M]^+$: calcd., 868.0080; found, 868.0140.

Note: To further elucidate the mechanism of formation of compound **5**, 2,2,6,6-tetramethylpiperidin-1-yl)oxyl (TEMPO) was added to the above described reaction. While **3** was consumed in a similar time-frame to the original conditions as evidenced by thin-layer chromatography, none of the pyrazinophane product, **5**, was observed at any time. Additionally, the gelatinous solid observed as a byproduct under the original reaction conditions was not observed upon addition of TEMPO. This indicates that both **5** and the uncharacterized polymer may be formed via a radical-based mechanism.

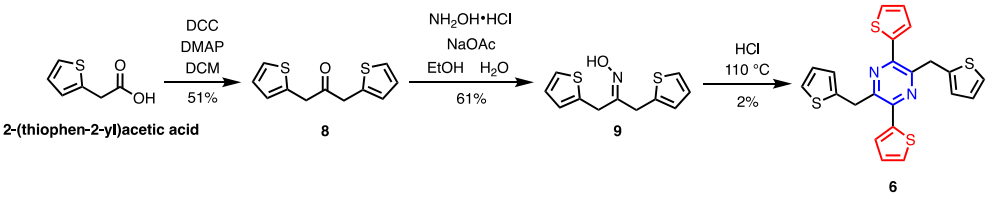

1,3-dithiophenylacetone (**8**)

Compound **8** was synthesized from 2-thiopheneacetic acid according to a previously reported procedure in 51% yield.[18]

Compound **9**

A suspension of hydroxylamine hydrochloride (3.91 g, 56.28 mmol), and sodium acetate (5.77 g, 70.35 mmol) in 80% aqueous EtOH (160 mL) was stirred at room temperature for 30 min. To this solution, 1,3-dithiophenylacetone (**8**, 7.82 g, 35.17 mmol) was added and the reaction mixture was heated to a gentle reflux for 1 h. After the completion of reaction by TLC, the reaction was cooled to room temperature and the solvent was removed via rotary evaporation. The obtained residue was purified by column chromatography (hexanes to ethyl acetate gradient) as eluent to obtain the oxime **9** in 61% yield. (Note: NMR peaks are split by the asymmetric hydroxyl group placement under the conditions used.) ^{1}H NMR (500 MHz, $CDCl_3$) δ 8.69 (bs, 1H), 7.21 (dd, J = 5.1, 1.2 Hz, 1H), 7.17 (dd, J = 5.2, 1.2 Hz, 1H), 6.97 (dd, J = 5.2, 3.4 Hz, 1H), 6.93 (dd, J = 5.2, 3.4 Hz, 1H), 6.87 (dd, J = 3.5, 1.1 Hz, 1H), 6.84 (dd, J = 3.5, 1.1 Hz, 1H), 3.91 (d, J = 1.0 Hz, 2H), 3.73 (d, J = 0.9 Hz, 2H). ^{13}C NMR (126 MHz, $CDCl_3$) δ 157.41, 138.58, 137.58, 127.23, 126.99, 126.75, 126.71, 124.98, 124.66, 33.64, 26.70. Note: mass spectrometry was not obtained for compound **7** due to its fragility in even gentle mass spectrometric analysis.

Compound **6**

In a N_2-flushed 100 mL round-bottom flask, the oxime **9** (1.49 g, 6.29 mmol) was dissolved in diethyl ether (15 mL). Hydrogen chloride dissolved in diethyl ether (2M, 31.47 mL, 62.95 mmol) was then added and a green-white solid precipitated out. The solid was allowed to settle out and was isolated by pipetting out the supernatant ether under

nitrogen, and removing trace volatiles first by N_2 flow, and then by applying a vacuum. The remaining solid was heated under nitrogen at 110 °C overnight. The reaction mixture was then purified by column chromatography (hexanes to ethyl acetate gradient) followed by recrystallization from chloroform to afford analytically pure compound **6** as off-white needle crystals (2%). ^{1}H NMR (500 MHz, $CDCl_3$) δ 7.52 (dd, *J* = 3.8, 1.1 Hz, 1H), 7.48 (dd, *J* = 5.1, 1.1 Hz, 1H), 7.21 (dd, *J* = 5.1, 1.2 Hz, 1H), 7.12 (dd, *J* = 5.1, 3.7 Hz, 1H), 6.95 (dd, *J* = 5.2, 3.5 Hz, 1H), 6.88 (dd, *J* = 3.5, 1.2 Hz, 1H), 4.64 (d, *J* = 1.1 Hz, 2H). ^{13}C NMR (126 MHz, $CDCl_3$) δ 147.28, 143.92, 142.07, 140.50, 129.17, 128.19, 127.86, 126.91, 125.84, 124.75, 36.06. MS (MALDI-TOF) for $C_{22}H_{16}N_2S_4$ $[M]^+$: calcd., 436.0196; found, 435.9913.

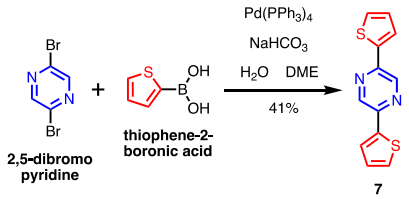

2,5-dithiophenylpyrazine (**7**)
Thiophene-2-boronic acid (1.61 g, 12.61 mmol), 2,5-dibromopyrazine (1.00 g, 4.20 mmol), and sodium bicarbonate (1.06 g, 12.61 mmol) were dissolved in a mixture of 1,2-dimethoxyethane (48 mL) and water (6 mL) under N_2. After refluxing the mixture for 1 hour, the solution was cooled below its boiling point and then tetrakis(triphenylphosphine)palladium(0) (0.224 g, 0.194 mmol) was added. After a further 24 hours of stirring at reflux, the reaction was cooled to room temperature, and the product was washed with water and extracted into chloroform. The combined organic layers were dried over $MgSO_4$, filtered, and concentrated *en vacuo*. Purification via silica-gel column chromatography (eluted with via a hexanes to dichloromethane gradient) followed by recrystallization from a hexanes/chloroform mixture afforded compound **7** as an off-white solid (41%). ^{1}H NMR (500 MHz, DMSO-d_6, 353K) δ 9.09 (s, 2H), 7.93 (dd, *J* = 3.6, 1.1 Hz, 2H), 7.73 (dd, *J* = 5.0, 1.1 Hz, 2H), 7.24 (dd, *J* = 5.0, 3.7 Hz, 2H). ^{13}C NMR (126 MHz, DMSO-d_6, 353K) δ 146.15, 141.60, 140.00, 129.78, 129.13, 126.67. MS (MALDI-TOF) for $C_{12}H_8N_2S_2$ $[M]^+$: calcd., 244.0129; found, 243.9749.

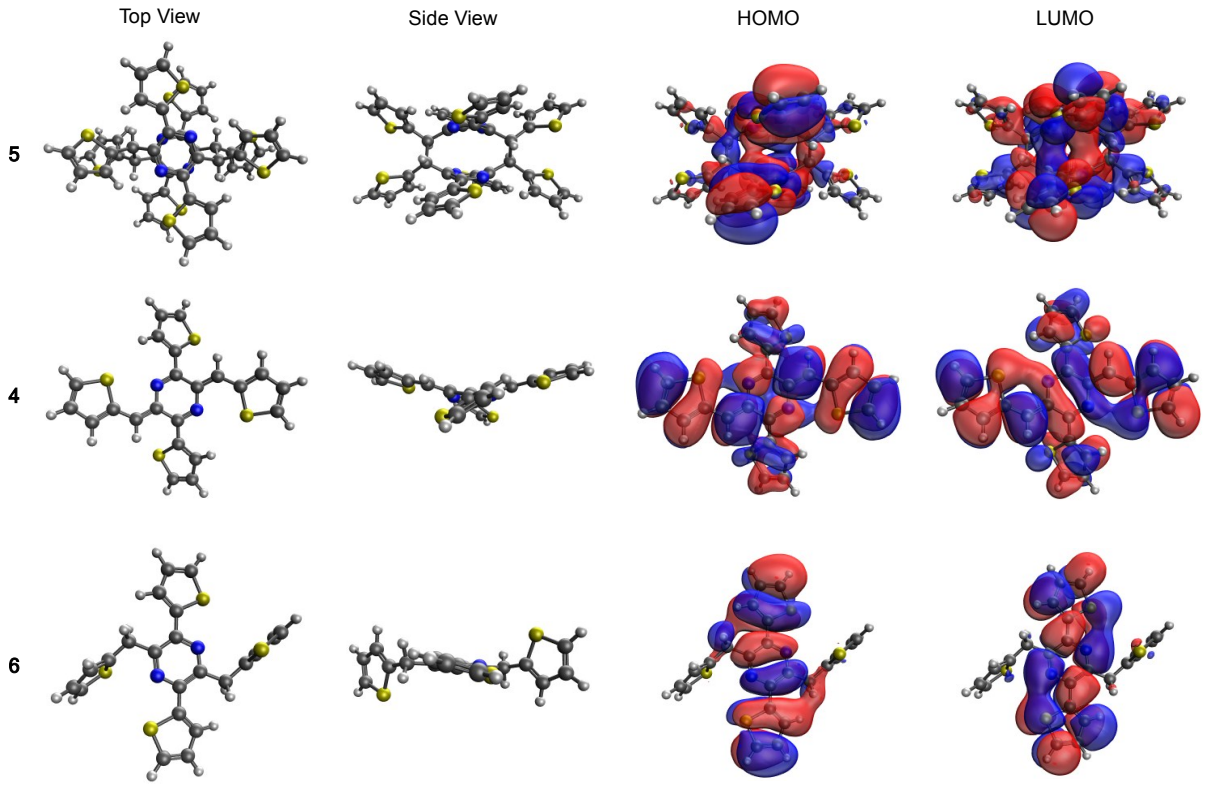

Figure S1. Results obtained from computations run using B3LYP/6-311++G**. Relaxed molecular geometry viewed normal to the AQM plane ("Top View") and from within the AQM plane ("Side View"), highest occupied molecular orbital orbital density map ("HOMO"), and lowest unoccupied molecular orbital orbital density map ("LUMO") for compounds **5**, **4**, and **6**.

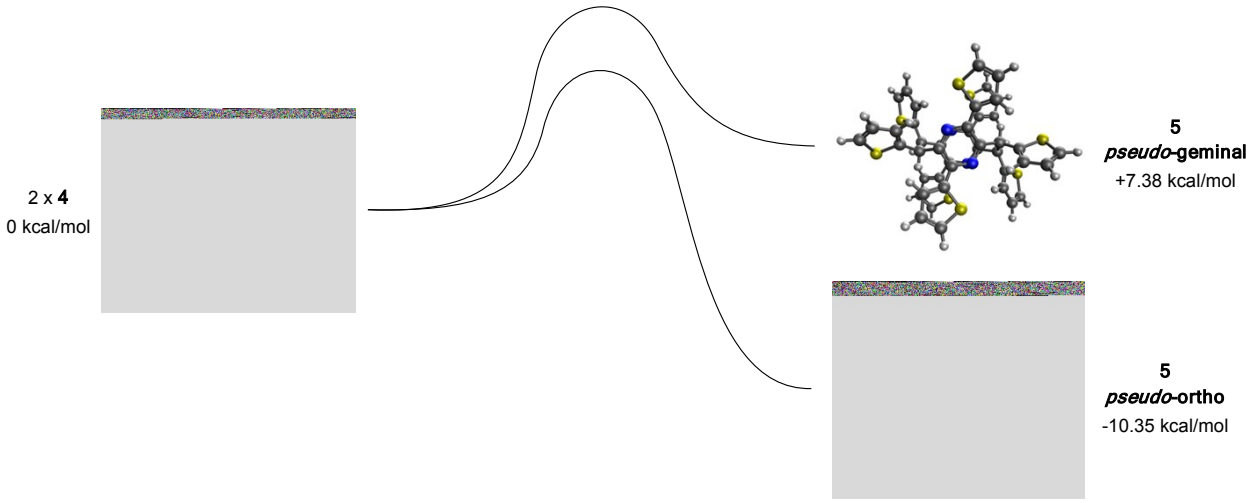

Figure S2. Schematic reaction energy pathways for the dimerization of **4** to produce either the *pseudo*-ortho or *pseudo*-geminal forms of **5**. Also shown are the ΔG^0 values obtained at the PBE0/6-31G* level employing *p*-xylene as the solvent relative to the total energy of the starting system with two molecules of **4**.

Compound	Conformer	E_e (kcal mol^{-1})	E_{e+t} (kcal mol^{-1})

Table S1. Relative energies calculated for the different conformers of compounds **5**, **6**, and **7** in the gas phase with respect to the most energetically favored conformer. E_e and E_{e+t} correspond to the electronic energy and electronic energy with thermal corrections (at 298.15 K) computed at the PBE0/6-31G* level of theory. Note: see corresponding images in Figure S3 below.

5	1	0.00	0.00
5	2	0.45	0.52
5	3	7.28	6.98
5	4	1.65	1.78
5	5	10.65	10.36
6	1	0.00	0.00
6	2	2.01	1.82
6	3	0.19	0.21
6	4	2.01	1.82
6	5	0.96	0.87
6	6	1.01	0.95
7	1	0.00	0.00
7	2	1.64	1.62
7	3	0.82	0.82

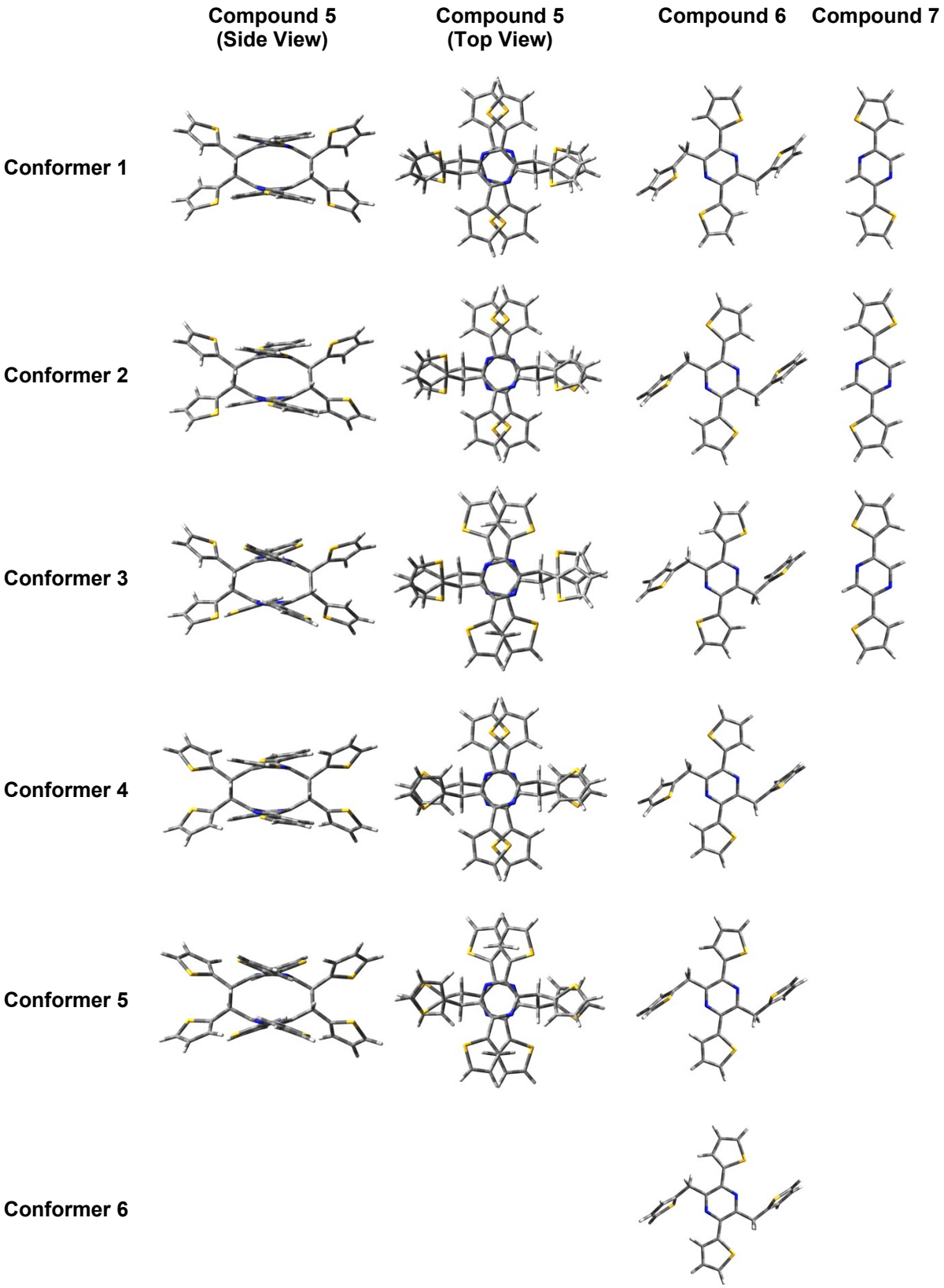

Figure S3. Conformers calculated for compounds **5**, **6**, and **7** at the PBE0/6-31G* level of theory in the gas phase. Note: see Table S1 for energies of each conformer.

Table S2. Most relevant vertical transition energies (E_{ab}^{calc}), oscillator strengths (*f*), and main components of the transitions (% Contribution), calculated at the TD-PBE0/6-31G* level of theory in dichloromethane solution.

Compound	E_{ab}^{calc} / eV (nm)	*Transition*	*f*	% Contribution
5	2.98 (416)	$S_0 \rightarrow S_1$	0.337	H→L (97)
5	3.37 (368)	$S_0 \rightarrow S_4$	0.581	H-1→L+1 (95)
5	3.80 (327)	$S_0 \rightarrow S_8$	0.348	H→L+2 (81)
6	3.41 (364)	$S_0 \rightarrow S_1$	0.865	H→L (98)
6	4.33 (286)	$S_0 \rightarrow S_5$	0.198	H→L+1 (87)
7	3.42 (362)	$S_0 \rightarrow S_1$	1.015	H→L (98)
7	4.12 (301)	$S_0 \rightarrow S_3$	0.143	H→L+1 (96)

Table S3. Energy calculated for the $S_1 \rightarrow S_0$ fluorescence emission transition (E_{em}^{calc}) at the TD-PBE0/6-31G* level of theory in dichloromethane solution.

Compound	E_{em}^{calc} / eV (nm)
5	1.39 (893)
6	3.01 (412)
7	3.06 (406)

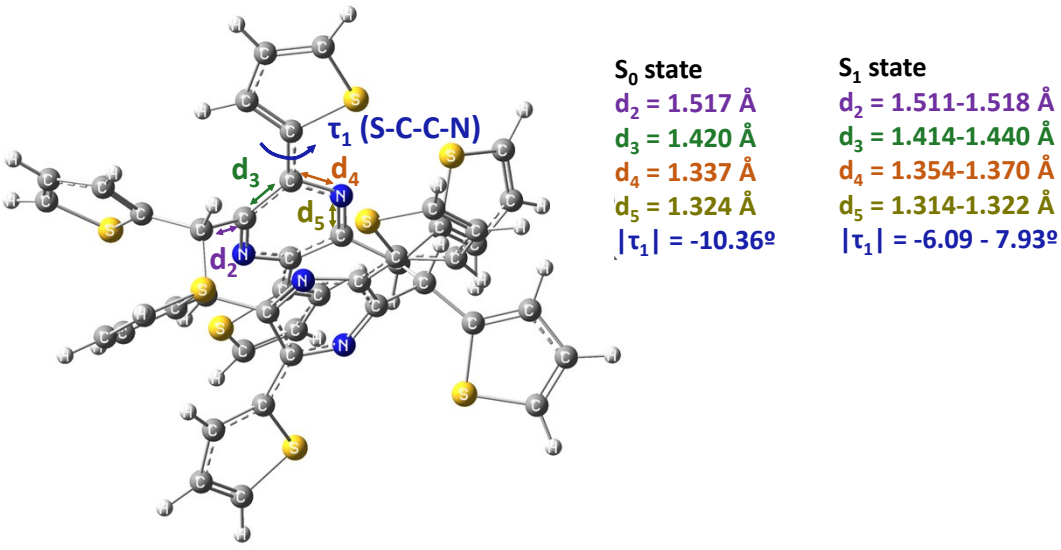

Figure S4. Some relevant bond lengths and intramolecular distances calculated for the dimer **5** in its S_0 and S_1 electronic states. The calculations were carried out at the PBE0/6-31G* level of theory employing dichloromethane as solvent.

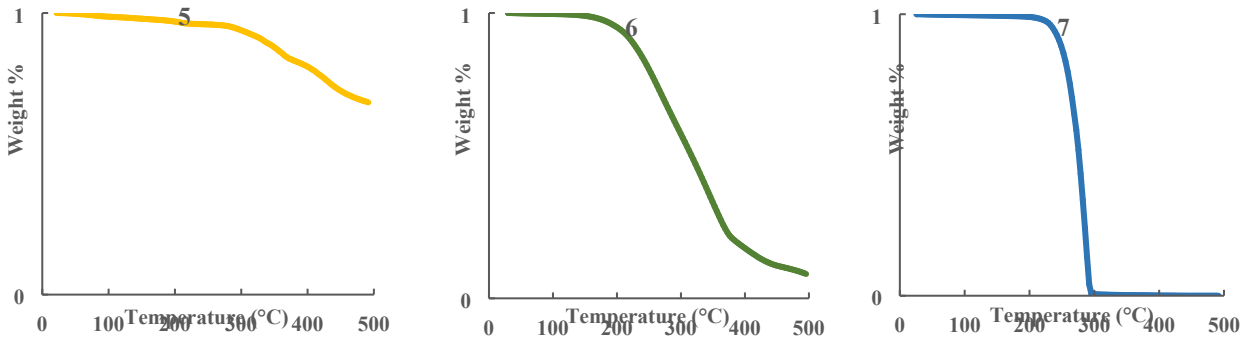

Figure S5. The thermogravimetric analysis traces obtained for compounds **5**, **6**, and **7**.

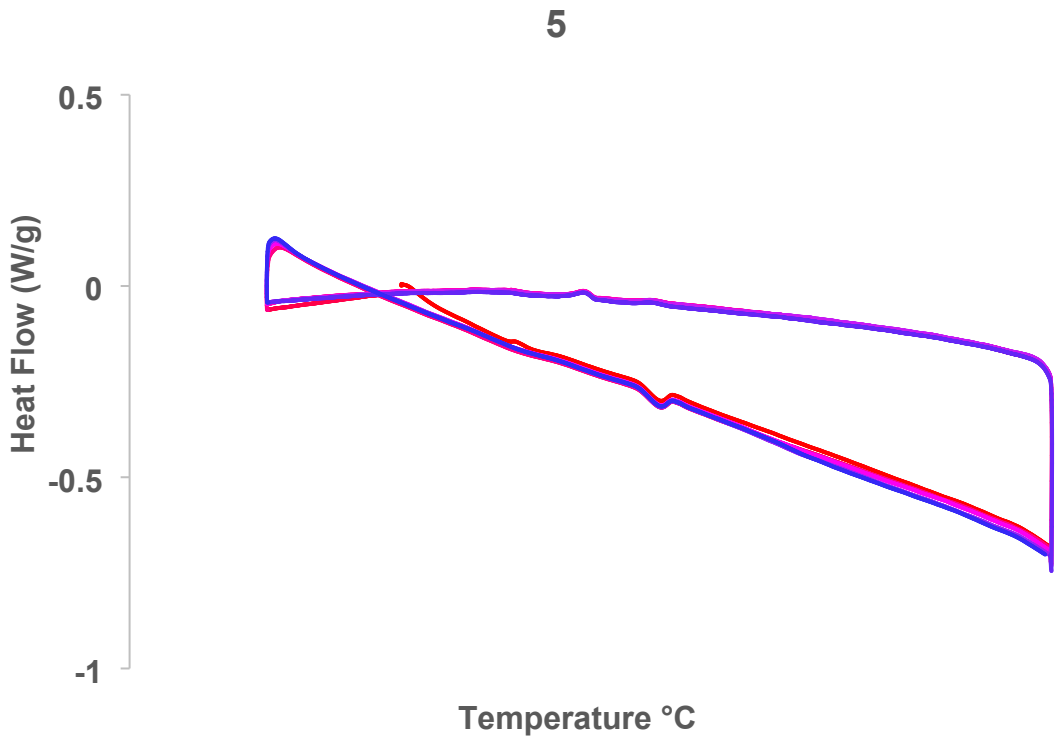

Figure S6. Differential scanning calorimetric trace obtained for compound **5** over five cycles of heating and cooling (shown in a gradient from red to blue, red being the first cycle).

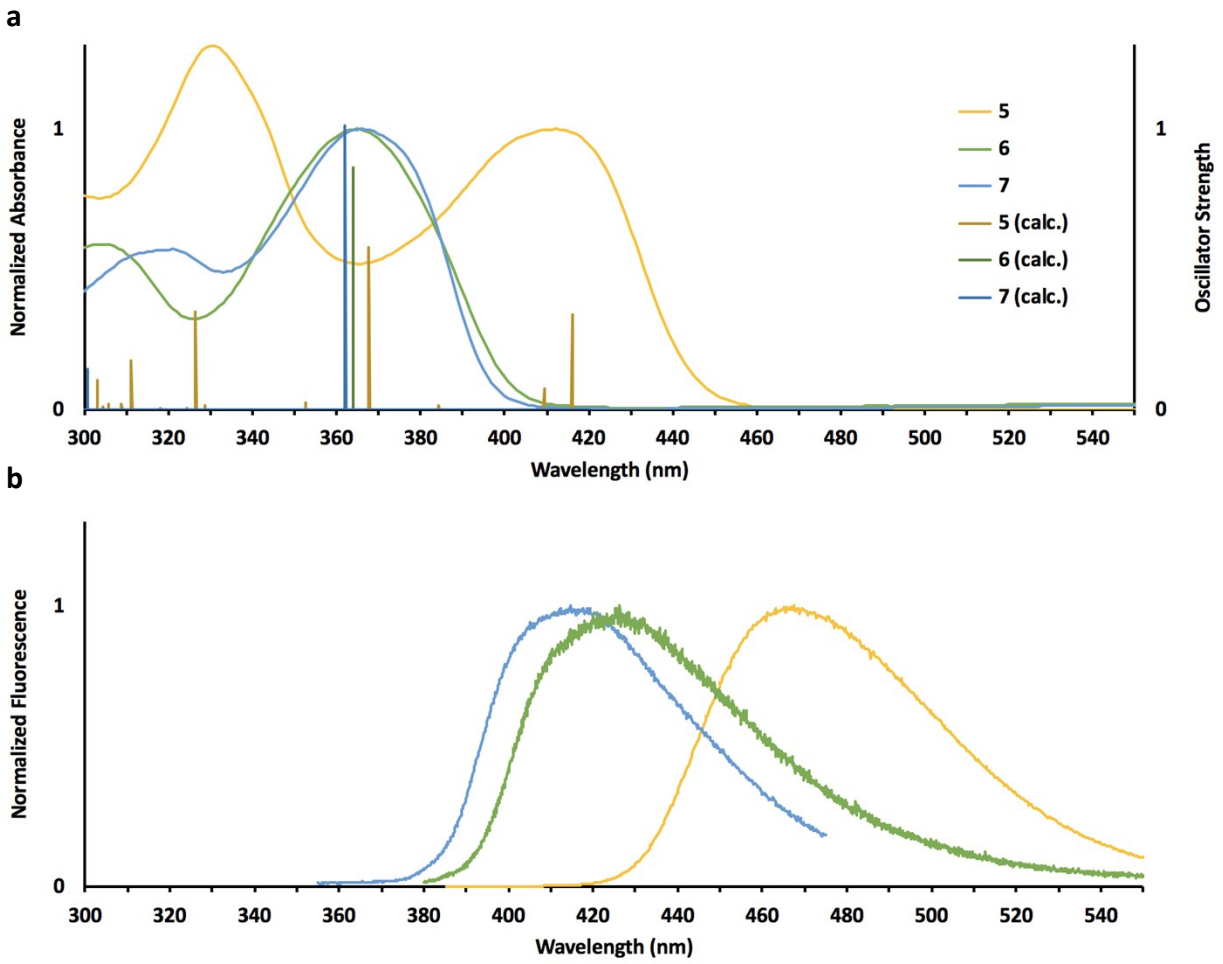

Figure S7. Optical properties of compounds **5** (yellow), **6** (green), and **7** (blue) in dilute dichloromethane solutions at 25 °C. (**a**) Normalized UV-Vis absorption spectroscopic traces for the three compounds superimposed over their respective calculated optical transitions (TD-PBE0/6-31G* in CH_2Cl_2). (**b**) Normalized fluorescence spectroscopic traces for the three compounds.

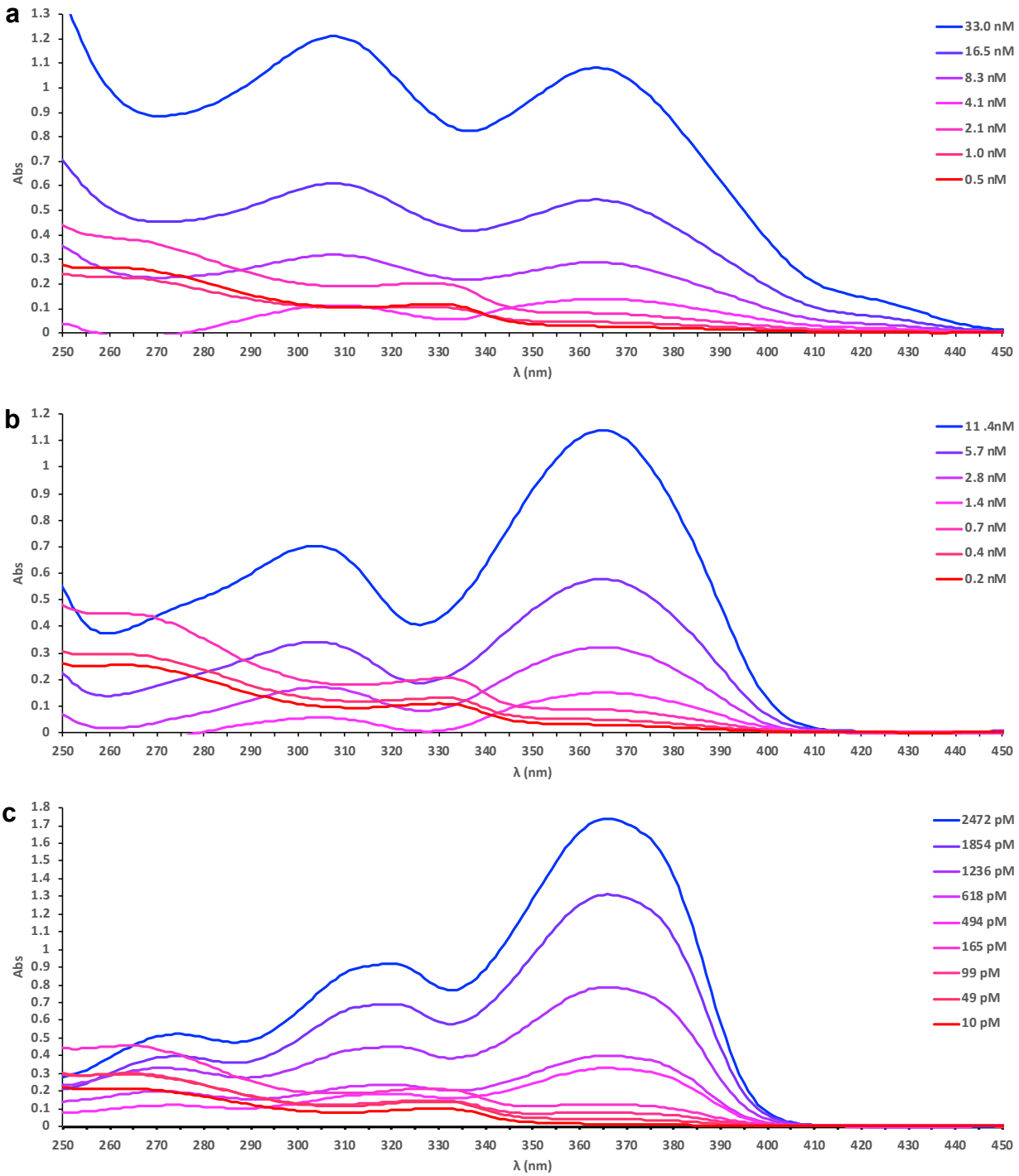

Figure S8. UV-Visible spectroscopic traces of (**a**) cyclophane **5**, (**b**) monomeric analog **6**, and (**c**) chromophore analog **7** at different concentrations in dichloromethane.

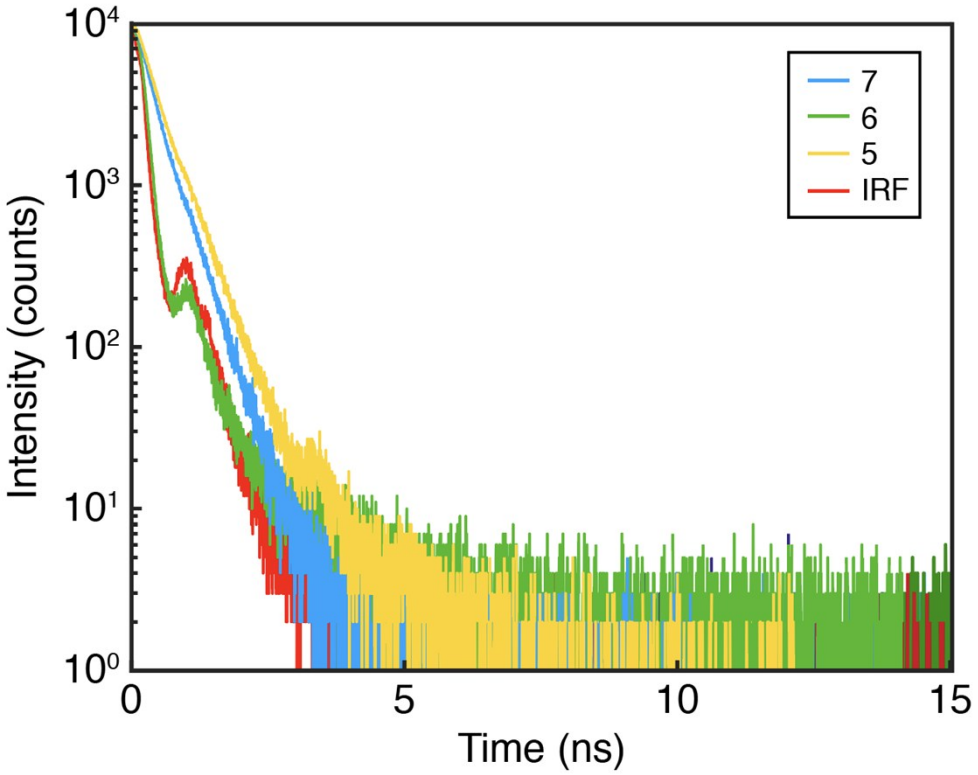

Figure S9. Fluorescence Lifetime Measurements Obtained for Compounds **5** (yellow, 0.43 ns), **6** (green, ≤ 0.14 ns), and **7** (blue, 0.37 ns) in dilute dichloromethane solutions at 25 °C. IRF (red, 0.10 ns) indicates the "instrument response function"—the shortest lifetime measurable on the particular instrument used. It can be seen that the lifetime calculated for compound **6** represents an upper bound, as it is very close to the IRF.

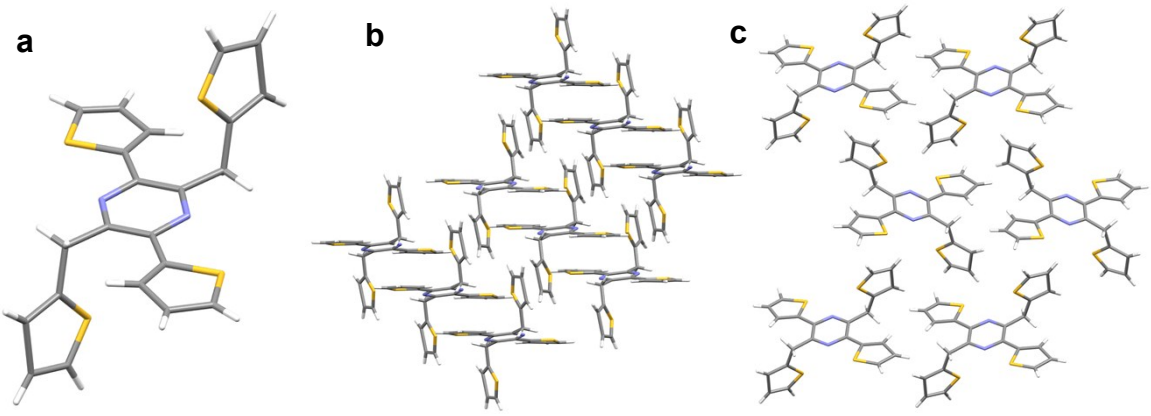

Figure S10. X-ray crystallographic structure of monomer analog **6**, showing (**a**) an isolated molecule and (**b** and **c**) molecular packing.

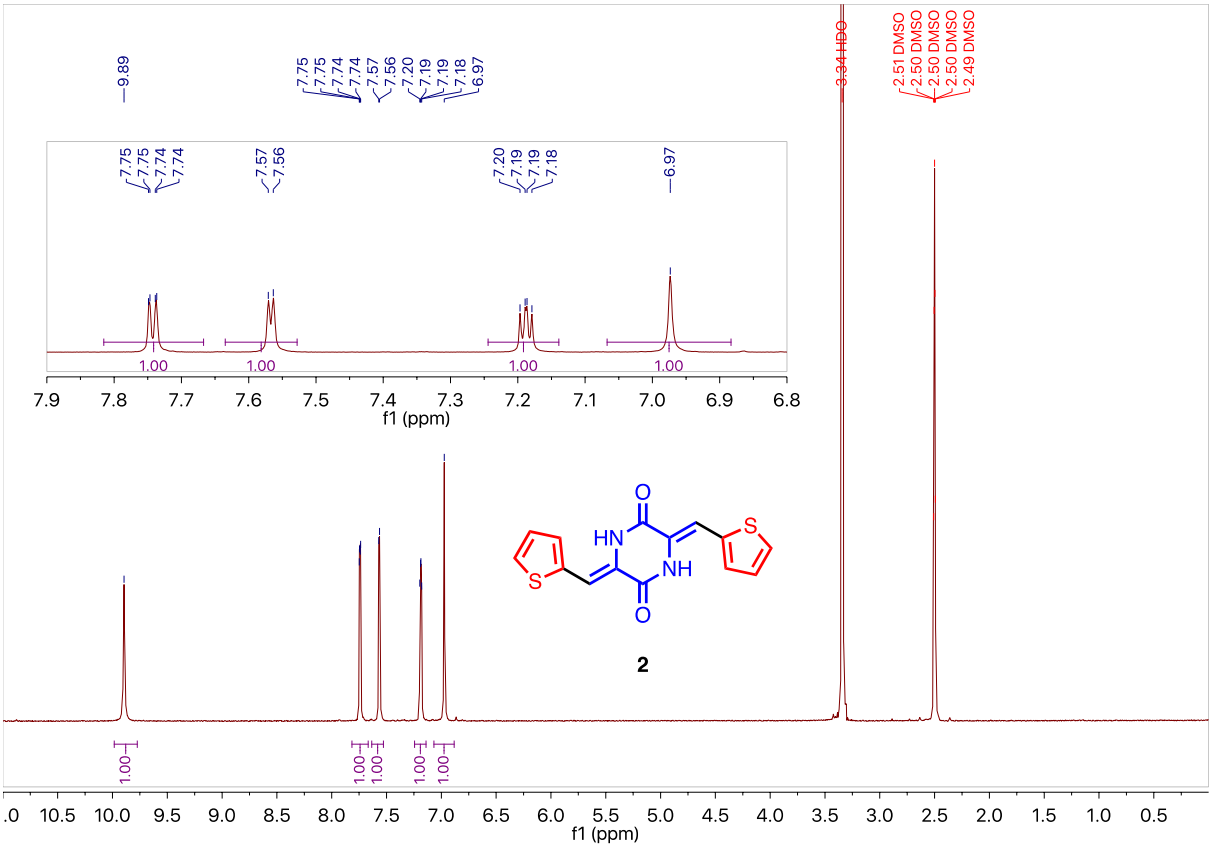

Figure S11. ^{1}H NMR Spectrum of **2** (DMSO-d6, 298K)

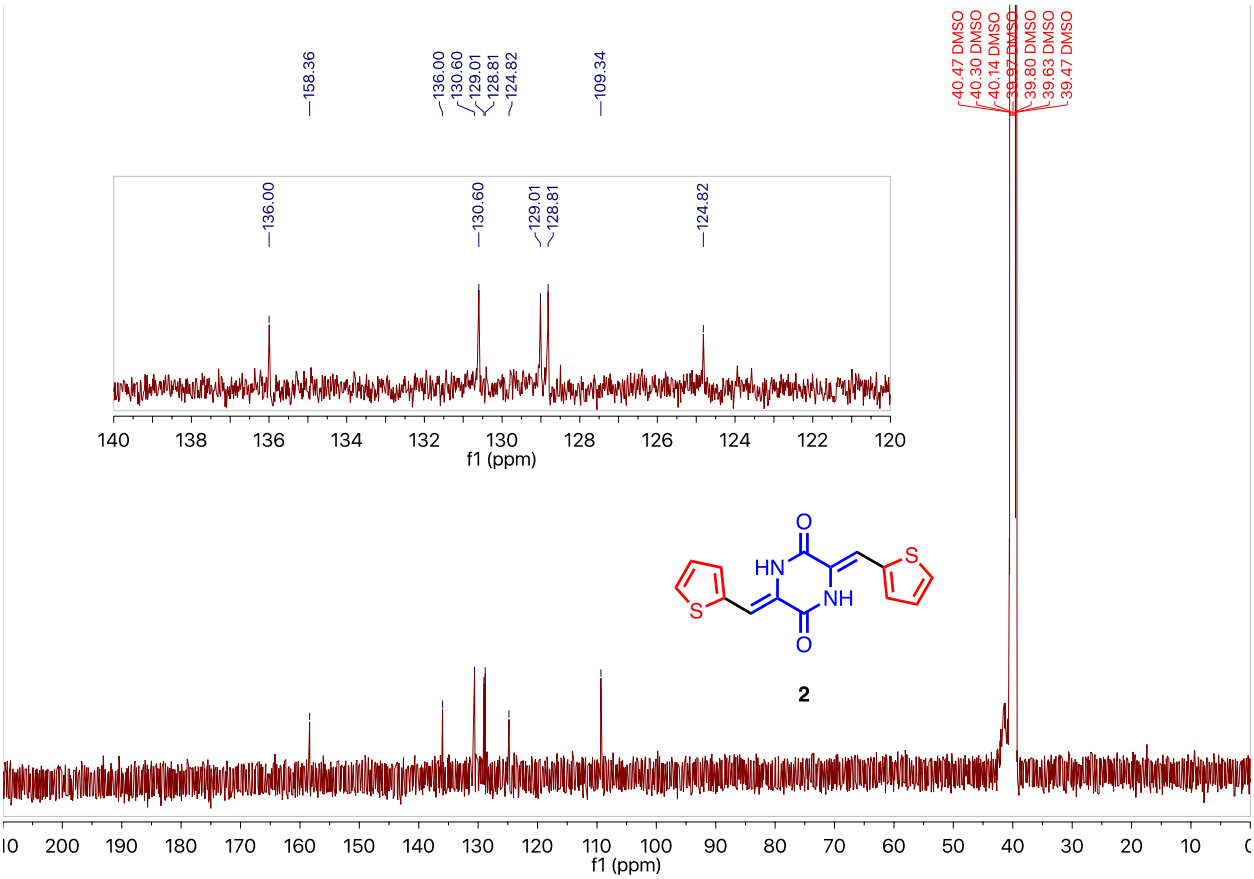

Figure S12. ^{13}C NMR Spectrum of **2** (DMSO-d6, 298K)

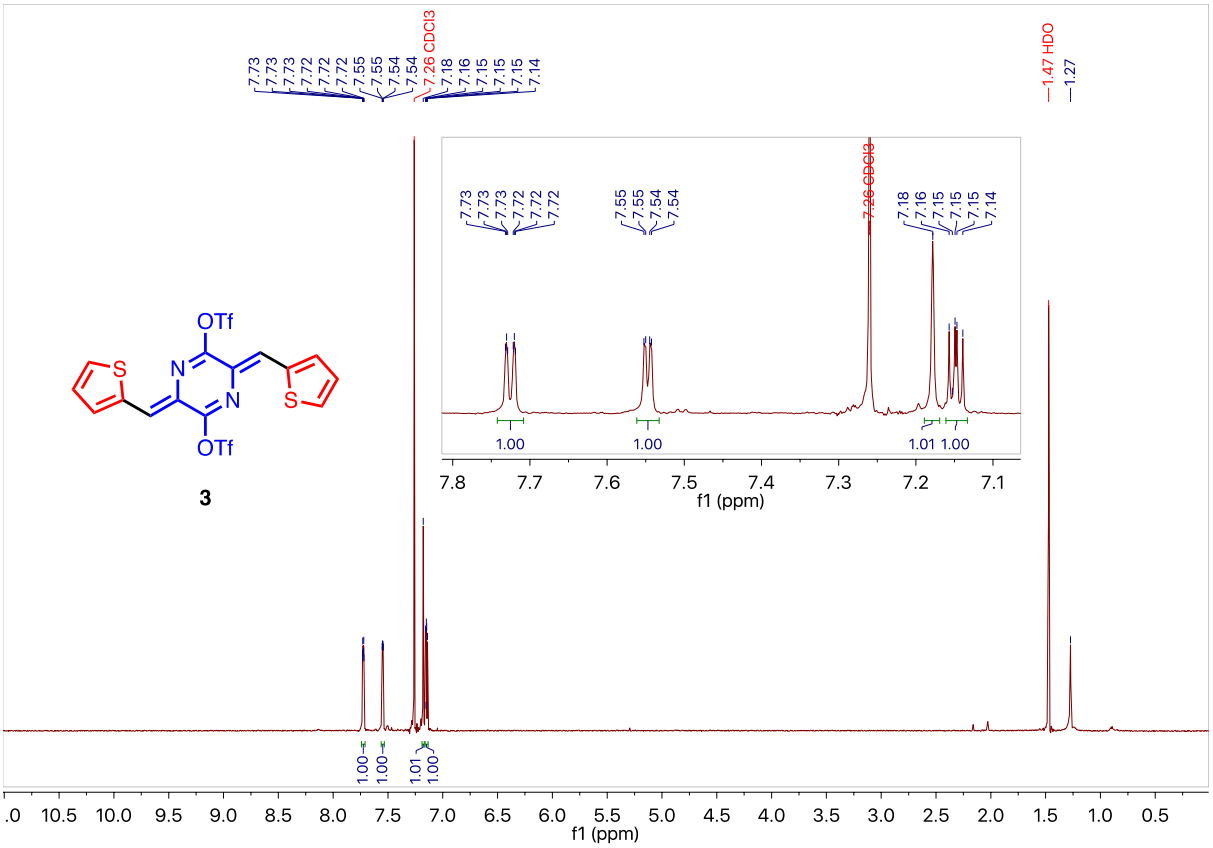

Figure S13. ^{1}H NMR Spectrum of **3** ($CDCl_3$, 323K).

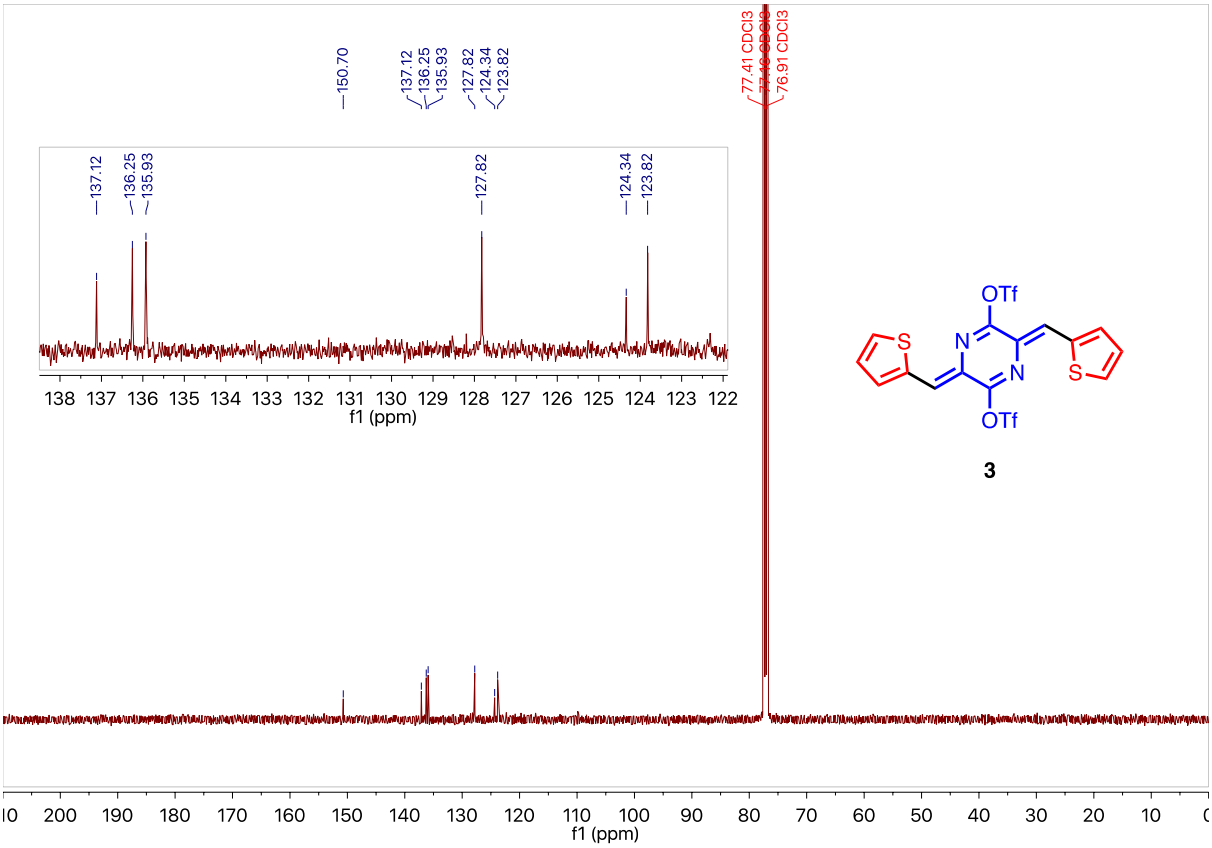

Figure S14. ^{13}C NMR Spectrum of **3** ($CDCl_3$, 323K).

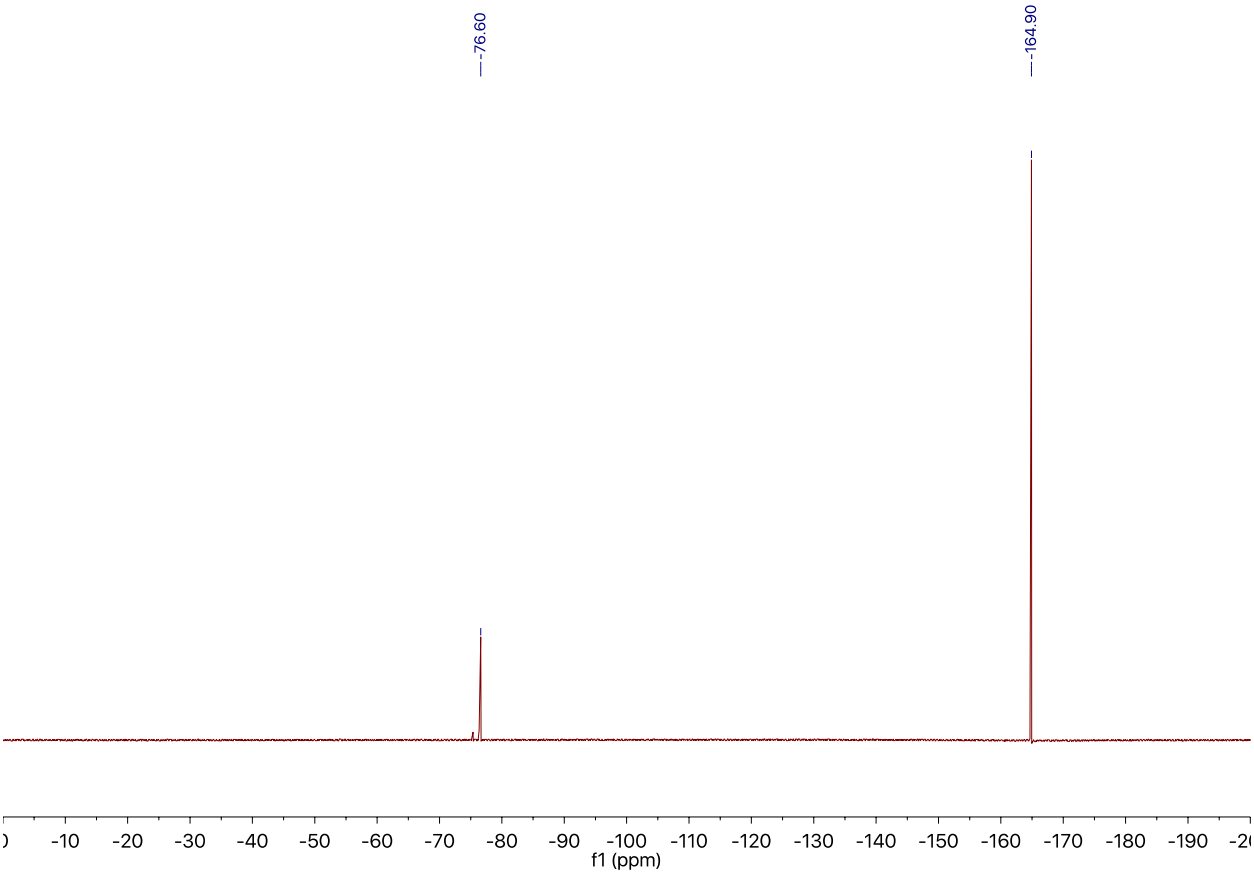

Figure S15. ^{19}F NMR Spectrum of ***3*** with hexafluorobenzene added as an internal standard (singlet set to -164.9 ppm) ($CDCl_3$, 273K).

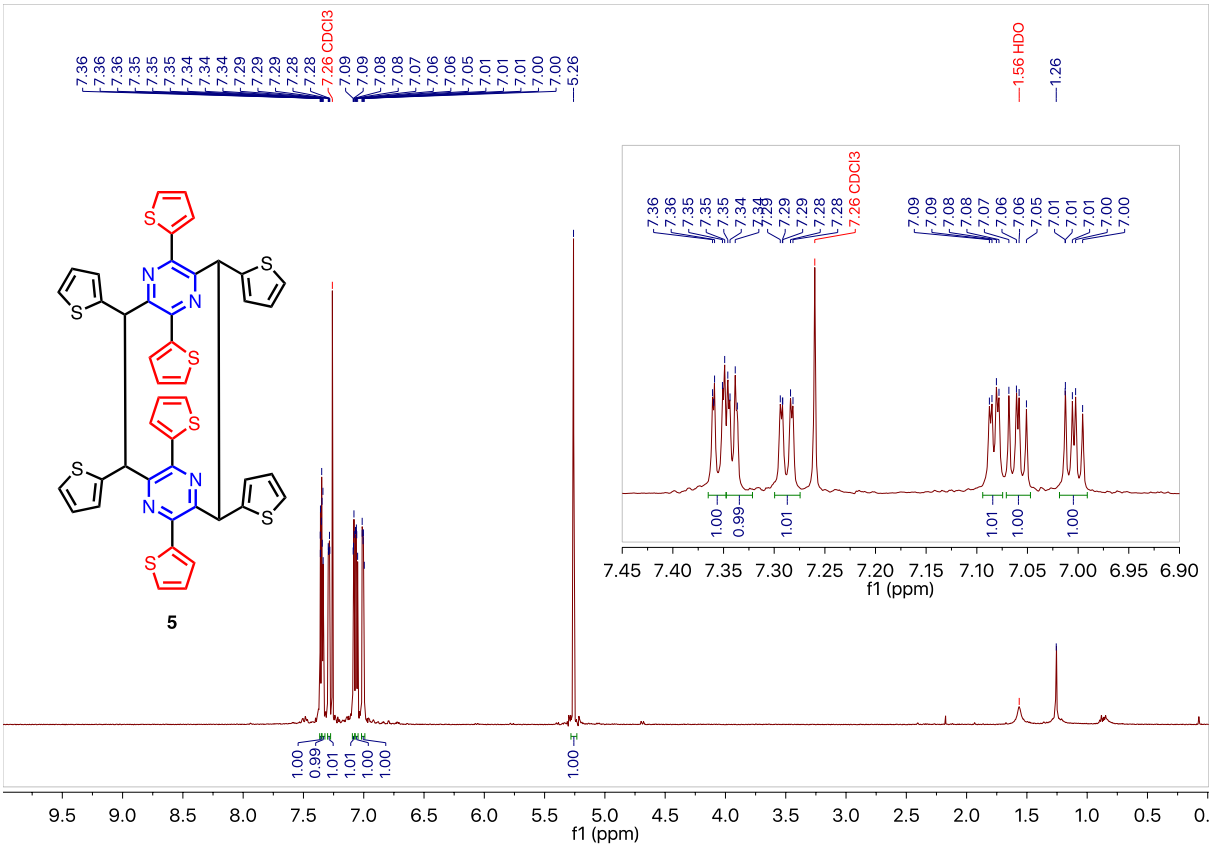

Figure S16. ^{1}H NMR Spectrum of **5** ($CDCl_3$, 298K).

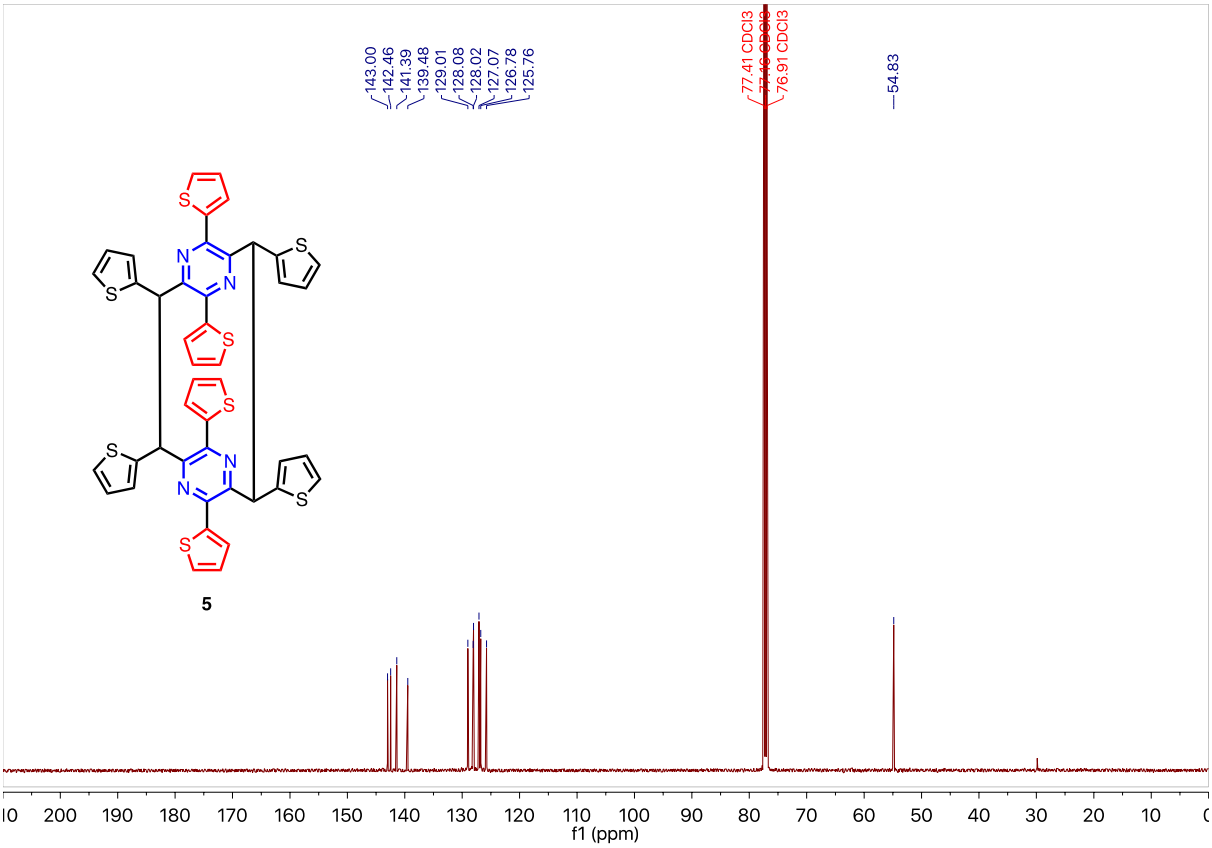

Figure S17. ^{13}C NMR Spectrum of **5** ($CDCl_3$, 298K).

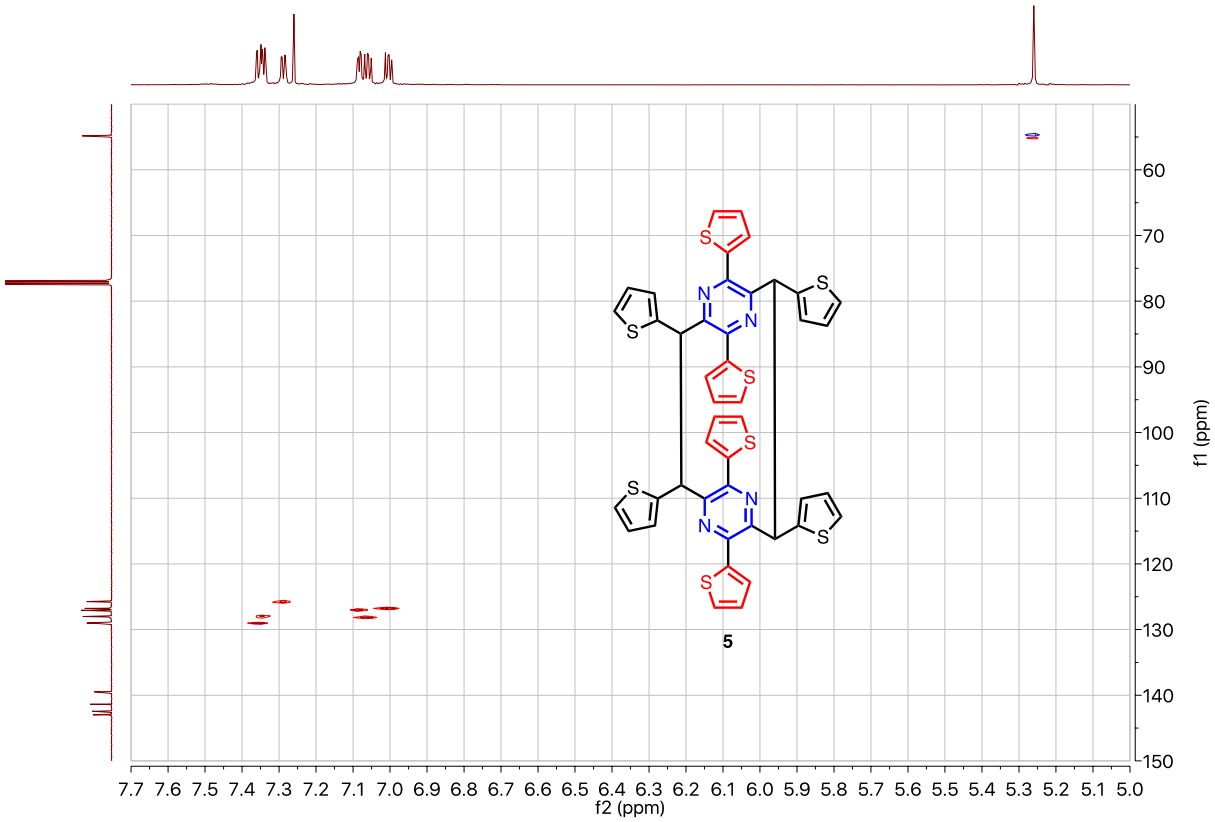

Figure S18. HMQC Spectrum of **5** ($CDCl_3$, 298K).

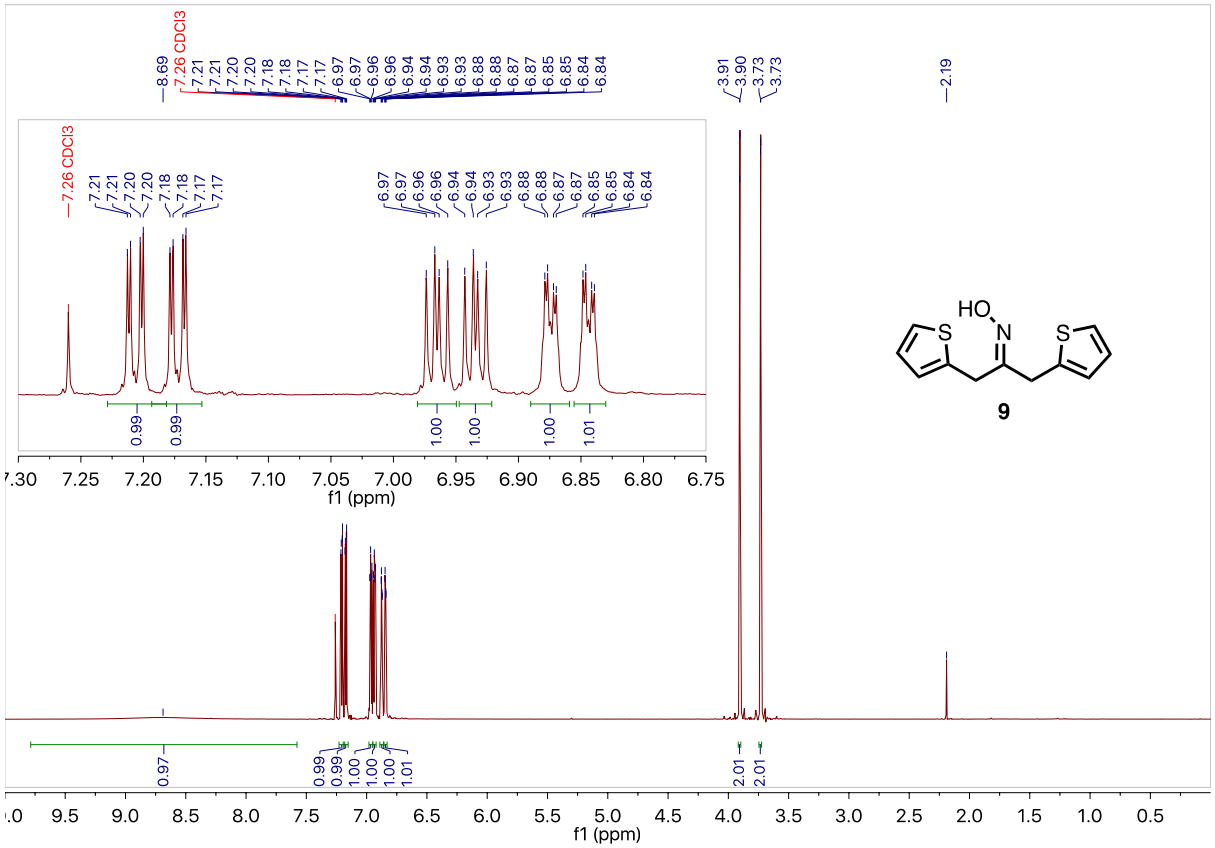

Figure S19. ^{1}H NMR Spectrum of **9** ($CDCl_3$, 298K).

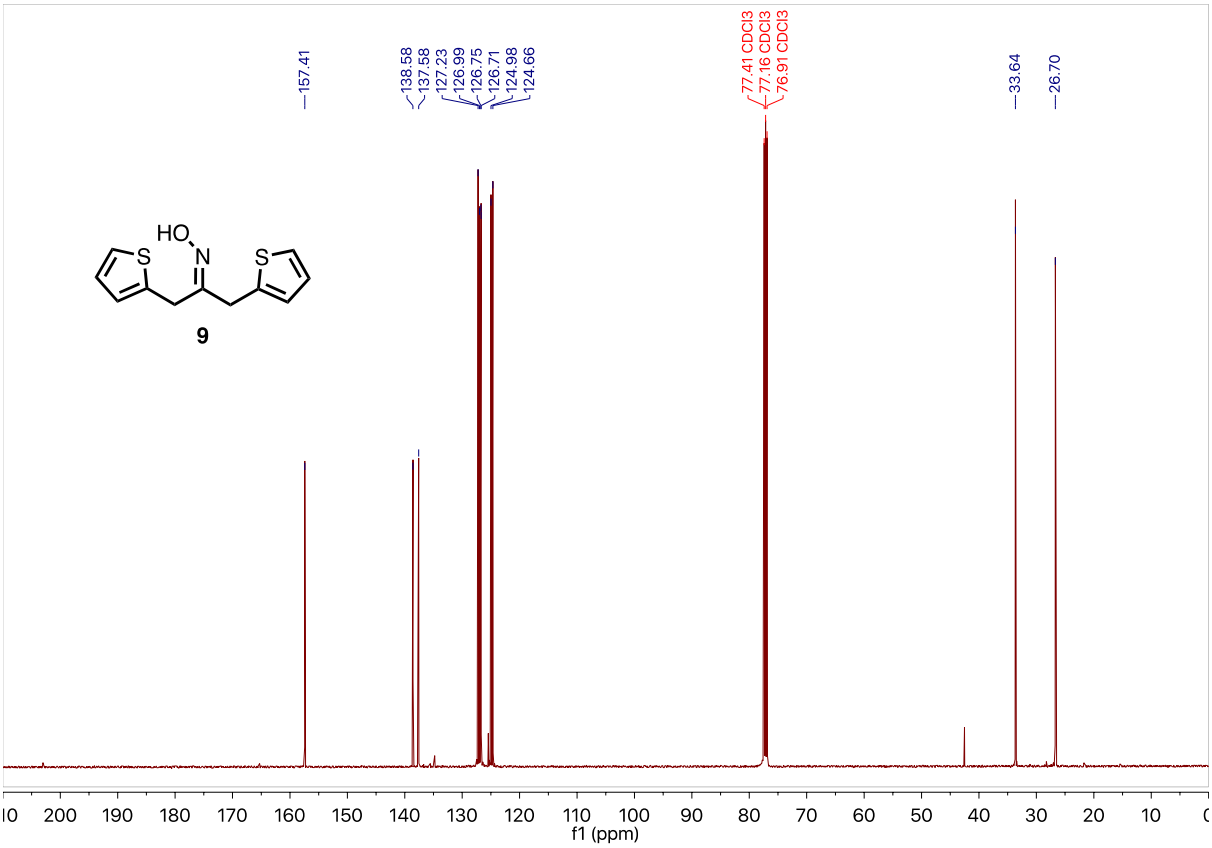

Figure S20. ^{13}C NMR Spectrum of **9** ($CDCl_3$, 298K).

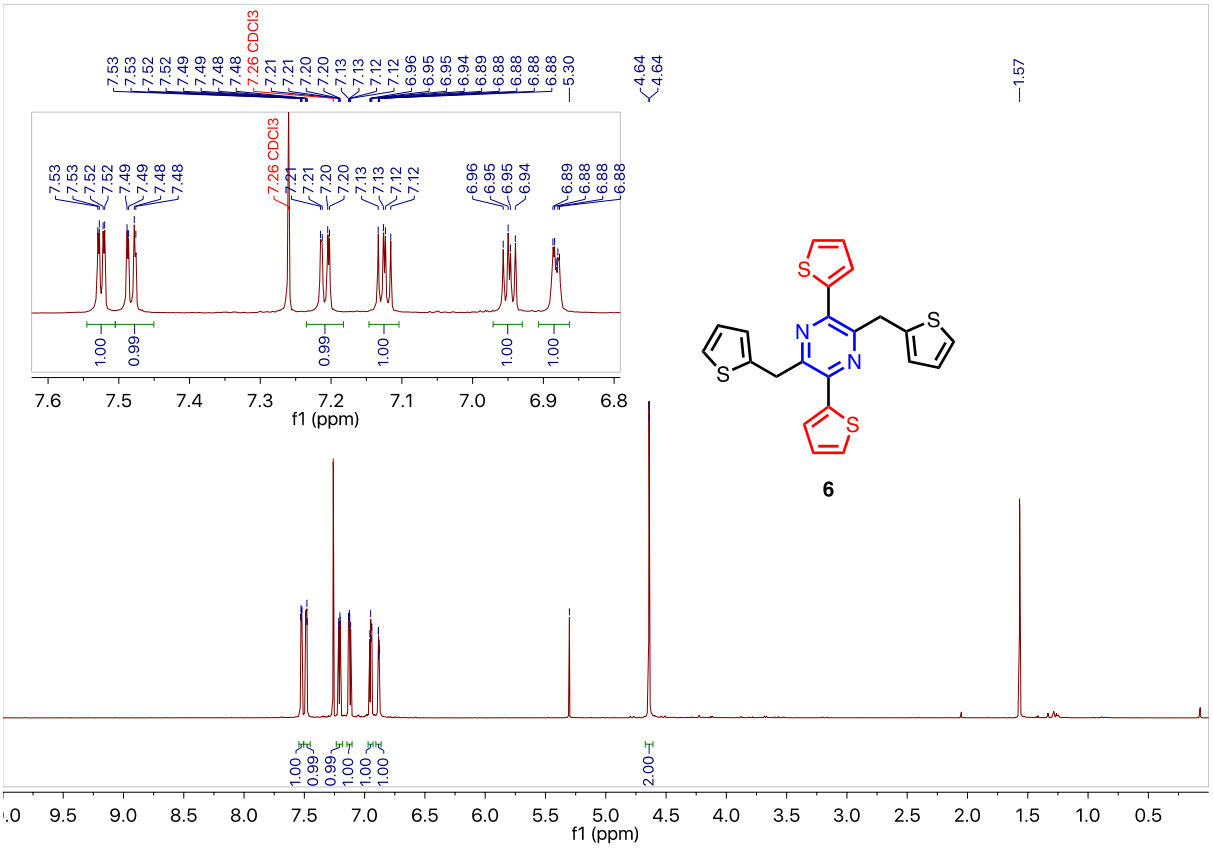

Figure S21. ^{1}H NMR Spectrum of **6** ($CDCl_3$, 298K).

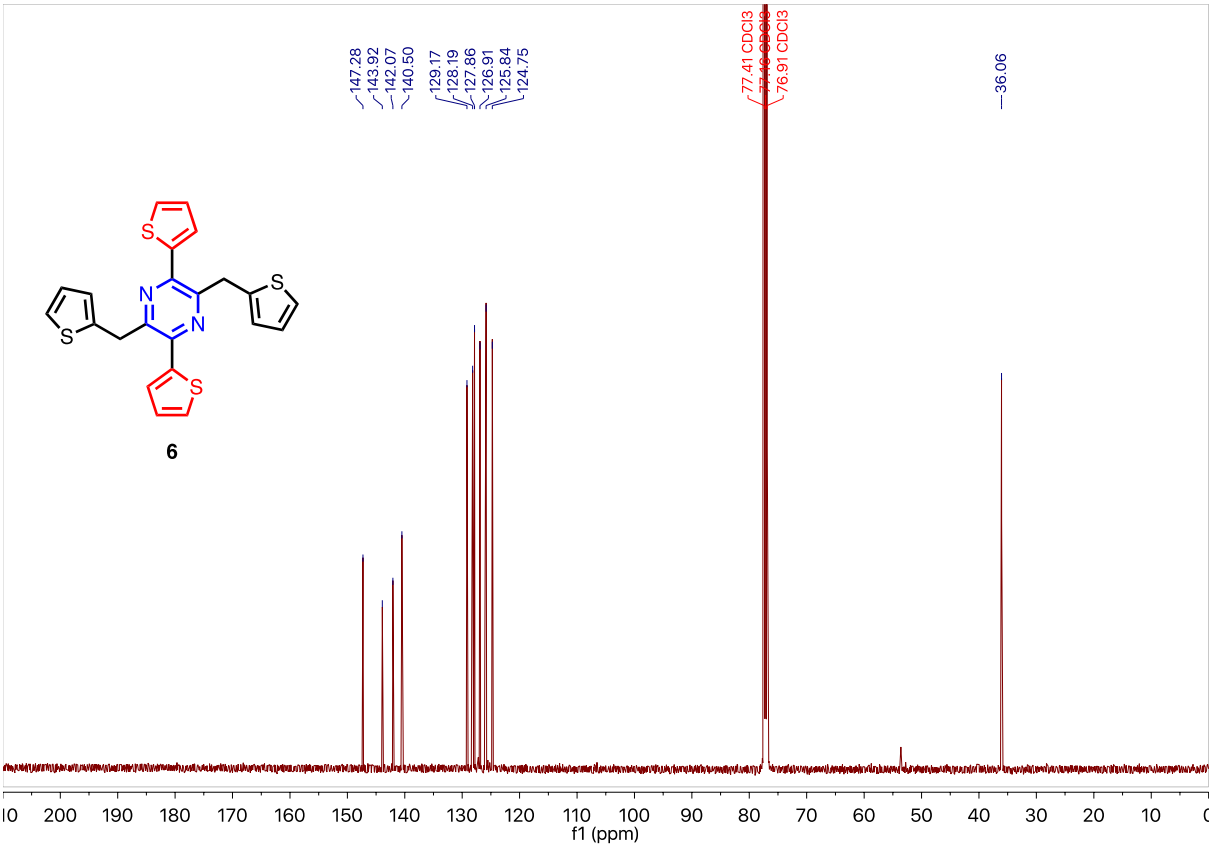

Figure S22. ^{13}C NMR Spectrum of **6** ($CDCl_3$, 298K).

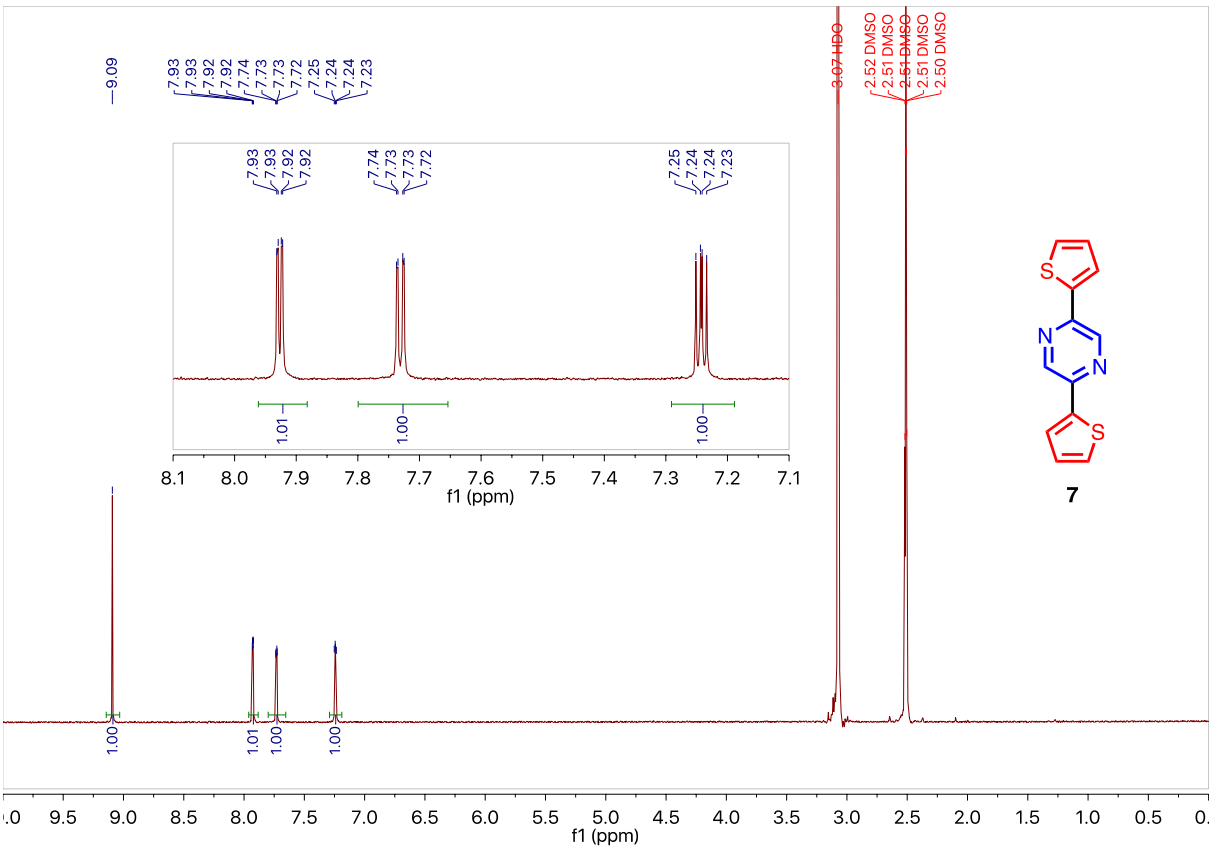

Figure S23. ^{1}H NMR Spectrum of **7** (DMSO-d_6, 353K).

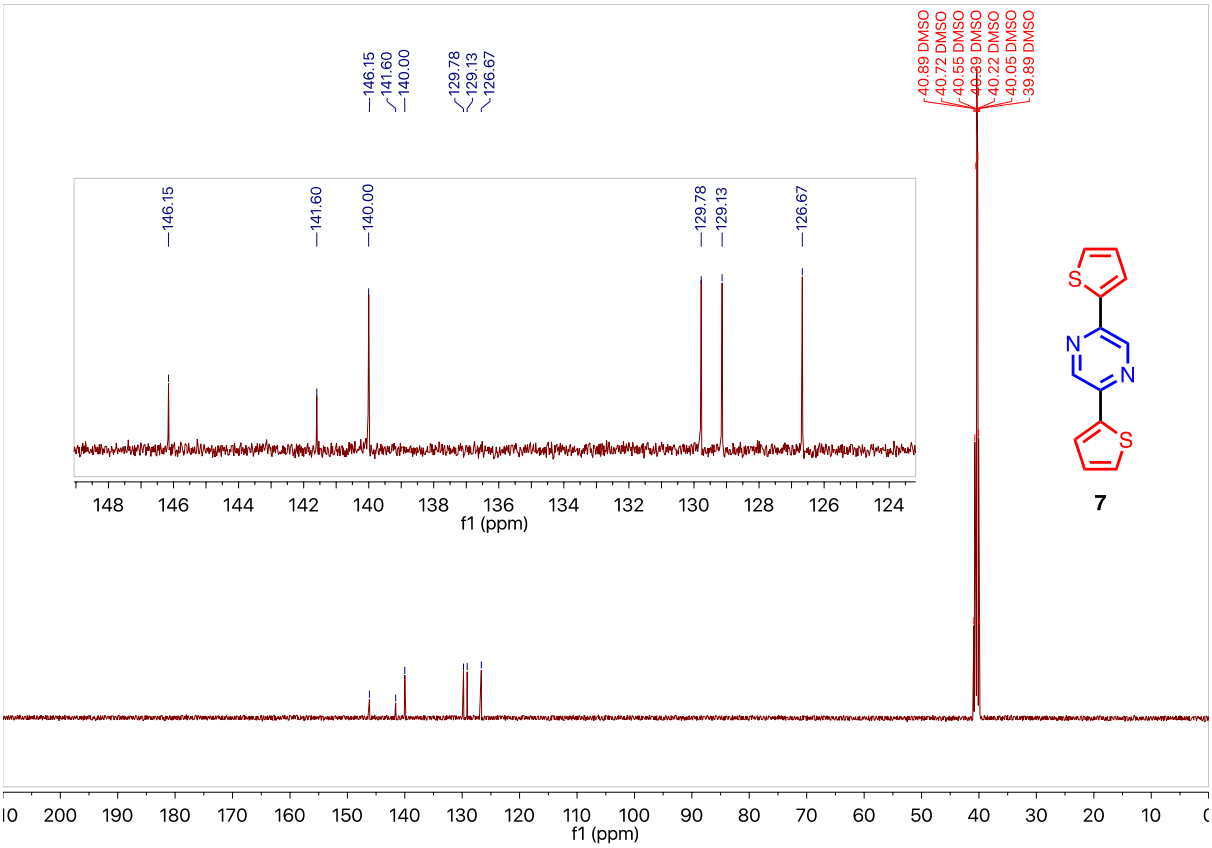

Figure S24. ^{13}C NMR Spectrum of **7** (DMSO-d_6, 353K) .

References

1. P. A. W. Dean and D. G. Ibbott, *Can. J. Chem.*, 1976, **54**, 177-187.
2. N. D. Bronstein, Y. Yao, L. Xu, E. O'Brien, A. S. Powers, V. E. Ferry, A. P. Alivisatos, R. G. Nuzzo, *ACS Photonics*, 2015**,** ***2***, 1576-1583.
3. Y. Shao, Z. Gan, E. Epifanovsky, A. T. B. Gilbert, M. Wormit, J. Kussmann, A. W. Lange, A. Behn, J. Deng, X. Feng, D. Ghosh, M. Goldey, P. R. Horn, L. D. Jacobson, I. Kaliman, R. Z. Khaliullin, T. Kuś, A. Landau, J. Liu, E. I. Proynov, Y. M. Rhee, R. M. Richard, M. A. Rohrdanz, R. P. Steele, E. J. Sundstrom, H. L. Woodcock, P. M. Zimmerman, D. Zuev, B. Albrecht, E. Alguire, B. Austin, G. J. O. Beran, Y. A. Bernard, E. Berquist, K. Brandhorst, K. B. Bravaya, S. T. Brown, D. Casanova, C.-M. Chang, Y. Chen, S. H. Chien, K. D. Closser, D. L. Crittenden, M. Diedenhofen, R. A. DiStasio, H. Do, A. D. Dutoi, R. G. Edgar, S. Fatehi, L. Fusti-Molnar, A. Ghysels, A. Golubeva-Zadorozhnaya, J. Gomes, M. W. D. Hanson-Heine, P. H. P. Harbach, A. W. Hauser, E. G. Hohenstein, Z. C. Holden, T.-C. Jagau, H. Ji, B. Kaduk, K. Khistyaev, J. Kim, J. Kim, R. A. King, P. Klunzinger, D. Kosenkov, T. Kowalczyk, C. M. Krauter, K. U. Lao, A. D. Laurent, K. V. Lawler, S. V. Levchenko, C. Y. Lin, F. Liu, E. Livshits, R. C. Lochan, A. Luenser, P. Manohar, S. F. Manzer, S.-P. Mao, N. Mardirossian, A. V. Marenich, S. A. Maurer, N. J. Mayhall, E. Neuscamman, C. M. Oana, R. Olivares-Amaya, D. P. O'Neill, J. A. Parkhill, T. M. Perrine, R. Peverati, A. Prociuk, D. R. Rehn, E. Rosta, N. J. Russ, S. M. Sharada, S. Sharma, D. W. Small, A. Sodt, T. Stein, D. Stück, Y.-C. Su, A. J. W. Thom, T. Tsuchimochi, V. Vanovschi, L. Vogt, O. Vydrov, T. Wang, M. A. Watson, J. Wenzel, A. White, C. F. Williams, J. Yang, S. Yeganeh, S. R. Yost, Z.-Q. You, I. Y. Zhang, X. Zhang, Y. Zhao, B. R. Brooks, G. K. L. Chan, D. M. Chipman, C. J. Cramer, W. A. Goddard, M. S. Gordon, W. J. Hehre, A. Klamt, H. F. Schaefer, M. W. Schmidt, C. D. Sherrill, D. G. Truhlar, A. Warshel, X. Xu, A. Aspuru-Guzik, R. Baer, A. T. Bell, N. A. Besley, J.-D. Chai, A. Dreuw, B. D. Dunietz, T. R. Furlani, S. R. Gwaltney, C.-P. Hsu, Y. Jung, J. Kong, D. S. Lambrecht, W. Liang, C. Ochsenfeld, V. A. Rassolov, L. V. Slipchenko, J. E. Subotnik, T. Van Voorhis, J. M. Herbert, A. I. Krylov, P. M. W. Gill and M. Head-Gordon, *Mol. Phys.*, 2015, **113**, 184-215.
4. A. K. Rappe, C. J. Casewit, K. S. Colwell, W. A. Goddard and W. M. Skiff, *J. Am. Chem. Soc.*, 1992, **114**, 10024-10035.
5. Frisch, M. J., Trucks, G. W., Schlegel, H. B., Scuseria, G. E., Robb, M. A., Cheeseman, J. R., Scalmani, G., Barone, V., Petersson, G. A., Nakatsuji, H., Li, X., Caricato, M., Marenich, A. V., Bloino, J., Janesko, B. G., Gomperts, R., Mennucci, B., Hratchian, H. P., Ortiz, J. V., Izmaylov, A. F., Sonnenberg, J. L., Ding, F., Lipparini, F., Egidi, F., Goings, J., Peng, B., Petrone, A., Henderson, T., Ranasinghe, D., Zakrzewski, V. G., Gao, J., Rega, N., Zheng, G., Liang, W., Hada, M., Ehara, M., Toyota, K., Fukuda, R., Hasegawa, J., Ishida, M., Nakajima, T., Honda, Y., Kitao, O., Nakai, H., Vreven, T., Throssell, K., Montgomery Jr., J. A., Peralta, J. E., Ogliaro, F., Bearpark, M. J., Heyd, J. J., Brothers, E. N., Kudin, K. N., Staroverov, V. N., Keith, T. A., Kobayashi, R., Normand, J., Raghavachari, K., Rendell, A. P., Burant, J. C., Iyengar, S. S., Tomasi, J., Cossi, M., Millam, J. M., Klene, M., Adamo, C., Cammi, R., Ochterski, J. W., Martin, R. L., Morokuma, K., Farkas, O., Foresman, J. B., Fox, D. J.: Gaussian 09. 2009: Wallingford, CT.
6. J. P. Perdew, K. Burke and M. Ernzerhof, *Phys. Rev. Lett.*, 1996, **77**, 3865-3868.
7. C. Adamo and V. Barone, *Chem. Phys. Lett.*, 2000, **330**, 152-160.
8. M. Cossi, N. Rega, G. Scalmani and V. Barone, *J. Comput. Chem.*, 2003, **24**, 669-681.
9. J. Tomasi, B. Mennucci and R. Cammi, *Chem. Rev.*, 2005, **105**, 2999-3094.
10. R. Cammi, S. Corni, B. Mennucci and J. Tomasi, *J. Chem. Phys.*, 2005, **122**, 104513.
11. D. Jacquemin, E. A. Perpète, G. E. Scuseria, I. Ciofini and C. Adamo, *J. Chem. Theory Comput.*, 2008, **4**, 123-135.
12. SAINT Software for CCD Diffractometers, Bruker AXS Inc., Madison, WI, 2014.
13. G. M. Sheldrick, SADABS, Bruker Analytical X-ray Systems, Inc., Madison, WI, 2000.
14. G. M. Sheldrick, *Acta Crystallogr. A*, 2015, **71**, 3-8.
15. G. M. Sheldrick, *Acta Crystallogr. A*, 2008, **64**, 112-122.
16. L.-M. Yang, W. Rong-Yang, A. T. McPhail, T. Yokoi and K.-H. Lee, *J. Antibiot.*, 1988, **41**, 488-493.
17. C. L. Anderson, N. Dai, S. J. Teat, B. He, S. Wang and Y. Liu, Angew. Chem. Int. Ed., 2019, 58, 17978-17985.
18. J. Arias-Pardilla, W. Walker, F. Wudl and T. F. Otero, *J. Phys. Chem. B*, 2010, **114**, 12777-12784.